High Strength Metal-Carbon Nanotube Composites

A. Goyal*, D.A. Wiegand**, F. J. Owens** and Z. Iqbal*

*New Jersey Institute of Technology, University Heights,
Newark, New Jersey 07102, USA, ag28@njit.edu, iqbal@njit.edu
**US Army Research, Development and Engineering Center, Picatinny,
New Jersey 07806, USA, donald.wiegand@us.army.mil, frank.owens1@us.army.mil

ABSTRACT

Uniform dispersion of pre-synthesized nanotubes in metal matrices is difficult to achieve, and there is substantial damage to the nanotubes during subsequent composite fabrication. The demonstration of an *in-situ* process involving chemical vapor deposition of single-wall and multi-wall carbon nanotubes into iron matrices without the concomitant formation of iron carbides is reported here. It was found that the yield strength of carbide-free iron-carbon nanotube composites increased up to 45% with about 1 wt % of infiltrated single wall carbon nanotubes (SWNTs), and 36% with ~1 wt % multiwall carbon nanotubes (MWNTs), relative to that of similarly treated pure iron matrices of the same piece density. Vickers hardness coefficients were also substantially enhanced - 74% and 96%, respectively, for composites with SWNTs and MWNTs relative to the metal matrices without nanotubes.

Keywords: metal composites, nanocomposites, chemical vapor deposition, carbon nanotubes, yield strength

1 INTRODUCTION

Carbon nanotubes have been extensively investigated for developing polymer matrix nanocomposites and a number of such nanocomposites are already being used in various applications [1]. Metallic composites, particularly those of iron and aluminum, containing carbon nanotubes would offer distinct advantages over polymeric composites, but the development of metal matrix composites remains in its infancy [2] in spite of its great potential, primarily because of high fabrication costs and difficulty in scaling up. In one study [3], 5% to 10 % by weight of pre-synthesized arc-grown multiwall carbon nanotubes were dispersed in aluminum matrices resulting in an increase of hardness, but no tensile strength measurements were performed. In another study [4], mechanical dampening characteristics of MWNT/magnesium composites formed by high pressure infiltration were studied and compared with that for the pristine metal matrix, but no significant improvement was observed. A detailed study was performed by Flahaut et al [5] using pre-synthesized nanotubes, which were then hot pressed with iron and Al_2O_3. The nanotubes suffered significant damage due to the high temperatures of around 1500-1600 ˚C used in this process and no substantial increase in mechanical properties was reported. Goh et al. [6] reinforced magnesium matrices with carbon nanotubes using powder metallurgy techniques and reported an increase of only 0.2% in yield strength and 0.18 % in ductility. Some of the issues which preclude mechanical property enhancement in metal-nanotube composites arise due to the high processing temperatures used in infiltrating pre-synthesized nanotubes into the metal matrix. Moreover, the methods used do not lead to good dispersion of the nanotubes in the metal matrix and efficient nanotube-metal contact and pinning. We have developed a scaleable chemical vapor infiltration technique [7, 8] which forms metal matrix nanocomposites with enhanced yield strength. Specifically, catalytic chemical vapor deposition was used to infiltrate metal matrices with single and multiwall carbon nanotubes using carbon monoxide and acetylene as carbon sources. Vickers hardness numbers and stress-strain curves were measured to characterize the mechanical properties of the composites formed.

2 EXPERIMENTAL

The catalyst and promoter precursors, iron acetate, cobalt acetate and molybdenum acetate, each 0.01 weight % of total solution, respectively, were dissolved in ethanol. Typically 3-5 gms of micron-sized iron powder was soaked in this solution, dried, and pressed into thin cylindrical pellets under an applied load of 5000 Kg. The pellets were 13 mm in diameter and between 4 and 5 mm in thickness with piece densities of 5.7 to 6.10 gm/cc. The average porosities of all the samples used in the mechanical measurements were the same. The catalyst loading in our samples was very low. The amount of catalyst metal in the iron matrix was estimated to be about 0.003 weight % of the total weight of the pellet.

The pellets were placed in a quartz boat in a horizontal quartz tube high temperature furnace. The quartz tube was pumped down to about 10^{-3} torr. In case of SWNTs, the reactor was back-filled with flowing pure hydrogen for 30 minutes to an hour to reduce the oxides to metals at 500ºC. In second step the carbon source, carbon monoxide (CO), was introduced at 700°C into the reactor at a flow rate of 100 standard cubic centimeters per minute (sccm) for 30 minutes-1 hour to deposit SWNTs within the matrix. In case of MWNTs a single step protocol involving heating to 800°C under flowing argon followed by switching the gas

NSTI-Nanotech 2008, www.nsti.org, ISBN 978-1-4200-8503-7 Vol. 1

flow to a mixed carbon source of acetylene, CO and argon with flow rates of 6, 100 and 300 sccm, respectively, at atmospheric pressure, was used. Reference pellets were prepared with the same weight of iron powder and applied load, followed by same thermal cycles used to grow SWNTs and MWNTs. After completion of the deposition, the system was allowed to cool to room temperature under flowing argon.

The characterization of the composites was carried out by micro-Raman spectroscopy, x-ray diffraction (XRD), and field-emission scanning electron microscopy (FE-SEM). Vickers hardness measurements were conducted on using a LECO micro-hardness tester (LM 700, LECO Corp.). A load of 10 Kgf (kilogram force) at ambient temperature with a dwell time of 5 seconds was selected, average values are reported. Stress-strain data were obtained in compression with a MTS servo hydraulic system operated at a constant displacement rate so as to give a strain rate of about 0.00004/sec.

3 RESULTS AND DISCUSSIONS

The representative micro-Raman spectra obtained using 632.8 nm laser excitation from the surface of the nanocomposites are shown in Figs, 1a-c. In Fig 1a clear evidence for the formation of SWNTs is provided by the appearance of the characteristic SWNT lines associated with the carbon-carbon bond tangential modes near frequencies of 1591 cm^{-1} and 1552 cm^{-1} (the latter appearing as a well-defined shoulder in the spectrum), and the lines at 190, 247, 259 and 279 cm^{-1} due to the radial breathing modes (RBMs) of individual tubes of different diameters. The line observed at 293 cm^{-1} is likely to be associated with Fe_2O_3 present as an impurity in the iron matrix. The diameters (d, nm) of the individual SWNTs can be determined from the RBM frequency ω. For bundled SWNTs: $d = (238/\omega)^{1.075}$ [9]. The broad line at 1327 cm^{-1} assigned to defects and amorphous carbon was found to be relatively weak. This indicated that rather defect-free SWNTs are formed with relatively little amorphous carbon present. In Figure 1 b-c the Raman spectrum does not show the relatively sharp radial breathing mode (RBM) lines that are indicative of SWNTs . The lines at 1323 cm^{-1} and 1581 cm^{-1} observed for samples prepared with acetylene mixed with carbon monoxide can be assigned to the disordered (D) and graphitic (G) modes of MWNTs [10]. Concomitant growth of iron carbide also occurs when acetylene alone is used as the carbon feed – this aspect will be covered in more detail later in the discussion of the XRD results.

In Figures 2 a-b the diameters of 10 to 20 nm estimated from the FE-SEM images are an order of magnitude larger than the individual SWNT diameters obtained from the RBM Raman frequencies, indicating that the SWNTs formed are bundled into "ropes". The individual iron particles are likely to be anchored in place by the nanotube bridges. It is estimated from the measured increase in weight after nanotube deposition that typically 1 weight % or 2.2 volume % of SWNTs are incorporated into the

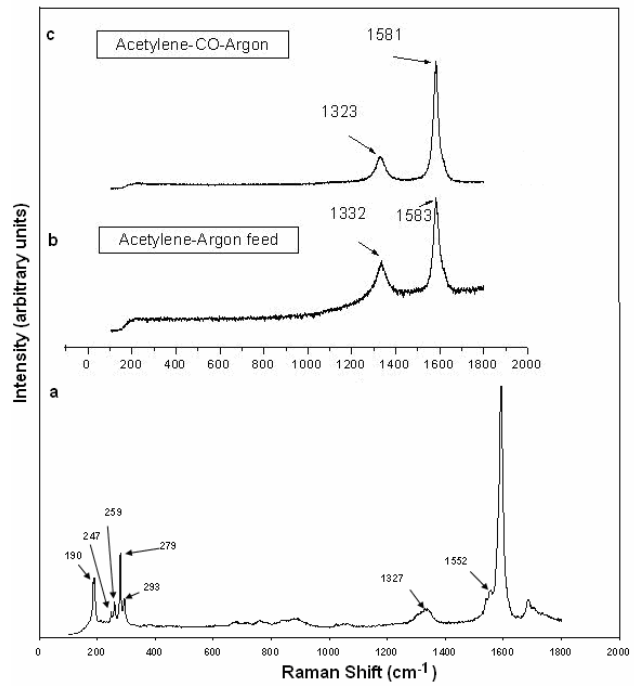

Figure 1: Raman spectra excited at 632.8 nm for: a) iron-SWNT, b) Iron-MWNT with acetylene feed, c) iron-MWNT with CO-acetylene feed.

starting iron matrix. FE-SEM images are consistent with largely MWNT formation, and the images shown in Fig. 2 c and d indicate somewhat denser growth of MWNTs compared to that of SWNTs. Fig. 2c depicts a low magnification image showing sizable MWNT penetration to a depth of 150 to 160 µm. A lower concentration of nanotubes is evident below 160 µm and through the approximately 0.5 mm thickness of the piece. A high magnification image taken from a region about 160 µm inside the top surface of the composite showing dense growth of MWNTs is displayed in Fig. 2d. Measured weight changes indicate a MWNT loading of up to 1 weight % ~ 4.48 volume % in the optimized iron-MWNT composites, which is similar to that obtained for the iron-SWNT composites.

XRD measurements (Fig. 3a) showed the presence of pure iron as indicated by reflections at 2θ values of 45, 65, 83, and 99 degrees. XRD reflections from SWNTs are not detected due to the relatively low weight % loading of SWNTs in the nanocomposites. Reflections associated with the iron-rich cementite Fe_3C phase were clearly absent. An XRD line at a 2θ value of 26 degrees was observed near the expected (001) reflection of graphite, but its intensity is too high for it to be attributed to a carbon phase. We tentatively assign this reflection to an iron sub-oxide formed in the iron matrix under our fabrication conditions. XRD patterns for the composites obtained using acetylene and argon, and a

mixture of acetylene, CO and argon, respectively, are shown in Fig. 3b and c. The XRD pattern for the composite prepared using acetylene and argon shows sharp reflections due to iron carbide, Fe_3C, while a mixture of CO, acetylene and argon is carbide free.

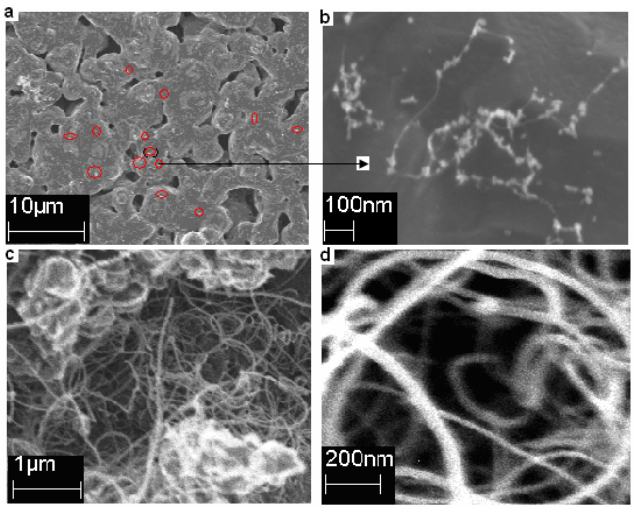

Figure 2: SEM images a) low magnification iron-SWNT, b) higher resolution SWNTs, c-d) MWNTs dispersed in iron matrix.

In order to understand why iron carbides are not formed when acetylene is mixed with CO, we propose the following sequence of reactions during *in-situ* growth with acetylene. The Fe_3C impurity phase is formed by reaction 1 below:

$$3Fe_2O_3 + 8H_2 + C_2H_2 \rightarrow 2Fe_3C + 9H_2O \quad (1)$$

It involves the reduction of Fe_2O_3 which is typically present in the iron matrix as an impurity phase, by hydrogen (formed by the initial dissociation of acetylene) followed by the adsorption of carbon from acetylene decomposition. The dissociation of acetylene is further enhanced by the presence of iron as catalyst. Iron is supersaturated with carbon and leads to the formation of iron carbide. Introducing CO initiates the occurrence of concurrent reactions 2 and 3 below. The presence of CO results in the formation of carbon nanotubes and CO_2 following the disproportionation reaction 2 in the presence of catalysts and reaction 3. In addition to that, reaction 3 scavenges hydrogen to form carbon nanotubes and prevents the reduction of Fe_2O_3 to Fe_3C via reaction 1.

$$2CO \rightarrow C + CO_2 \quad (2)$$
$$CO + H_2 \rightarrow C + H_2O \quad (3)$$

The above reaction sequence is consistent with the XRD data, which shows no evidence for the formation of the Fe_3C phase when CO is introduced into the carbon precursor feed.

Compressive stress-strain curves from two representative samples, with and without nanotubes show significant differences. The flow stress, the stress for the

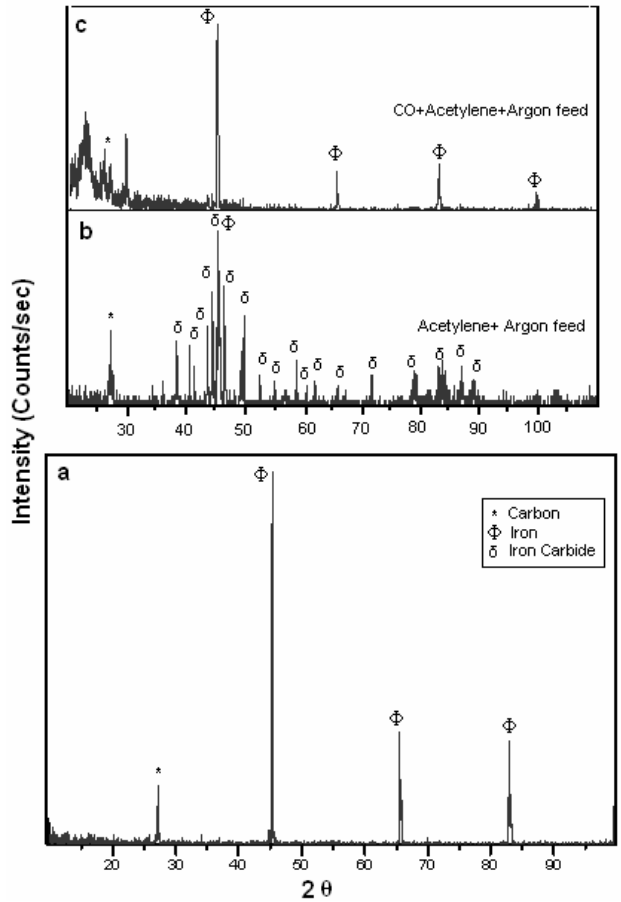

Figure 3: XRD a) iron-SWNT pellet, b) iron-MWNT pellet with acetylene feed, c) iron-MWNT with CO-acetylene.

significant plastic flow, is taken at the intersection of a straight line passing through the initial linear part of the stress-strain curve at low strains and a straight line passing through the linear work hardening part of the curve at larger strains. For the data in Fig. 4a, the flow stress is about 45% higher for the sample containing the SWNTs compared to the value for the reference iron sample. This flow stress is numerically equivalent to a yield stress obtained by a 0.4% strain offset technique. In addition, the work hardening coefficient, the slope in the latter linear part of the stress-strain curve at larger strains, is greater by a factor of about 3.4 (a 240% increase) for the sample containing the SWNTs relative to the reference sample. Thus, the mechanical strength of the sample containing SWNTs is significantly increased and much greater work is required to deform this sample plastically in the work hardening range. Since mechanical properties depend on porosity, it is important to emphasize that the porosity of the reference sample and the sample with SWNTs is the same and therefore differences in porosity cannot account for the enhanced mechanical strength. A sample was grounded by 170 µm on both sides and compression tests were repeated.

NSTI-Nanotech 2008, www.nsti.org, ISBN 978-1-4200-8503-7 Vol. 1

A stress-strain curve taken after grinding again indicates that the flow stress increased by an amount consistent with the work hardening during the initial compressions. Thus, the removal of the thin surface layers containing the highest densities of SWNTs had a minimal effect on the flow stress. These results indicate that the higher flow stresses observed in the samples containing the SWNTs are due to bulk effects and further that the SWNTs are distributed throughout the samples of thicknesses of the order of 0.6 cm. In case of MWNTs, the increase in upper and lower yield strength is 36 and 43% respectively as shown in Fig. 4 b. The lower yield point for the reference sample is at 179 MPa and for the iron-MWNT sample it is at 253.3 MPa. The upper yield point for the reference sample is at 200 MPa and at 276 MPa for the iron-MWNT composite.

The observed increase in strength of the nanotube-iron composites can be attributed to the mechanical support provided within the cavities by the nanotubes. The SWNTs are largely concentrated in cavities in the matrix as indicated by the FE-SEM images shown in Fig. 2. It is well-known that iron is an excellent catalyst towards nanotube growth [11] and can partially dissolve and bond to carbon to provide supporting bridges at the cavities. Bonding might also occur at nano-sized catalysts embedded in the larger iron particles of the matrix. Because of this support additional dislocation pinning may not be necessary. High porosity decreases mechanical strength because the average stress inside the material is greater than the average applied stress [12-13]. Providing support in the pores will lower the average stress in the material, which determines dislocation motion and yield. Thus yield will occur at higher values of the applied stress.

Overall this support at the cavities will offset in part the effect of the cavities in weakening the iron matrix, resulting in higher mechanical strength. The very large increase in the work hardening coefficient or slope suggests that the mechanism of work hardening may be different in the samples containing SWNTs than in the reference samples. For example, if the work hardening of the reference sample of Fig. 4 is due to long range dislocation-dislocation interactions, then the much higher work hardening slope of the sample containing SWNTs may be due to dislocation pile up at barriers introduced by the treatment which this sample received. When these barriers are SWNTs, it is expected that they are located not only in the cavities, but also distributed throughout the iron matrix.

Vickers hardness indices correlate with the tensile strength and fatigue resistance [14]. Typical average values of the Vickers hardness (HV) indices HV/10 (with 10 Kgf) of 95.2 for the reference sample and 135.7 for iron-SWNT sample showed an increase in the hardness index by 74%. For the carbide free iron-MWNT composites Vickers numbers showed enhancement in average hardness by 97.5%, which is substantially higher than that of an iron-SWNT composite with a similar concentration of nanotubes.

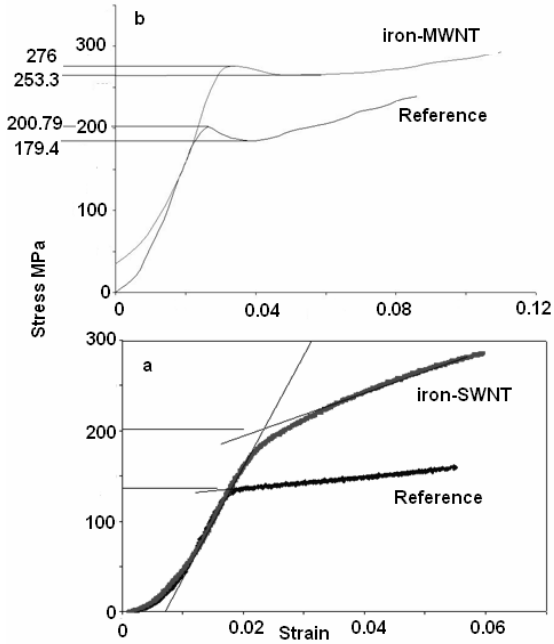

Figure 4: Compressive stress-strain curves for a) iron-SWNT and b) iron-MWNT composite.

REFERENCES

[1] A. Morgan, Material Matters 2, 20 (2007).

[2] P.K. Rohatgi and B. Schultz, Material Matters 2, 16 (2007).

[3] R. Zhong, H. Cong and P, Hou, Carbon, 41, 848, 2002

[4] J. Yang and R. Schaller, Mater. Sci. Eng. A. 370, 512, 2004

[5] E. Flahaut, A. Peigney, Ch. Laurent, Ch. Marlière, F. Chastel, A. Rousset, Acta Mater. 48, 3803, 2000.

[6] C.S. Goh, J. Wei, L.C. Lee, M. Gupta, Nanotechnology. 17, 7, 2006.

[7] A. Goyal, D. A. Wiegand, F. J. Owens and Z. Iqbal, J. of Mat. Res. 21, 522, 2006.

[8] A. Goyal, D. A. Wiegand, F. J. Owens and Z. Iqbal, Chem. Phys. Lett., 442, 365, 2007.

[9] L. Alvarez, A. Righi, S. Rols, A. Anglaret, J.L. Suavajol, E. Muñoz., W.K. Maser, A.M. Benito, M.T. Martínez, and G.F. de la Faunte, Phys. Rev. B. 63, 153401, 2001.

[10] C. Thomsen, S. Reich, H. Jantoljak, I. Loa, K. Syassen, M. Burghard, G.S. Duesberg, S.Roth, Appl. Phys. A. 69, 309, 1999.

[11] A.M. Cassell, N.R. Franklin, T.W. Tombler, E.M. Chan, J. Han and H. Dai, J. Am. Chem. Soc. 121, 7975, 1999.

[12] J.C. Wang, J. Mat. Sci. 19, 801, 1984.

[13] F.P. Knudsen, J. Am. Chem. Soc. 42, 376 (1959).

[14] W.D. Callister Jr.: Materials Science and Engineering: An Introduction, 6th ed. (John Wiley and Sons: New York, 2003), pp. 111-134.